

# **R-FUSE: Robust Fast Fusion of Multi-Band Images Based on Solving a Sylvester Equation - Complementary results and supporting materials**

Qi Wei, *Member, IEEE*, Nicolas Dobigeon, *Senior Member, IEEE*,  
Jean-Yves Tourneret, *Senior Member, IEEE*, José Bioucas-Dias, *Member, IEEE*  
and Simon Godsill, *Senior Member, IEEE*

## **TECHNICAL REPORT – 2016, July**

Department of Engineering, University of Cambridge  
Trumpington Street, Cambridge, CB2 1PZ, UK

### **Abstract**

This paper proposes a robust fast multi-band image fusion method to merge a high-spatial low-spectral resolution image and a low-spatial high-spectral resolution image. Following the method recently developed in [1], the generalized Sylvester matrix equation associated with the multi-band image fusion problem is solved in a more robust and efficient way by exploiting the Woodbury formula, avoiding any permutation operation in the frequency domain as well as the blurring kernel invertibility assumption required in [1]. Thanks to this improvement, the proposed algorithm requires fewer computational operations and is also more robust with respect to the blurring kernel compared with the one in [1]. The proposed new algorithm is tested with different priors considered in [1]. Our conclusion is that the proposed fusion algorithm is more robust than the one in [1] with a reduced computational cost.

### **Index Terms**

Multi-band image fusion, Woodbury formula, circulant matrix, Sylvester equation

Part of this work has been supported by the ERA-NET MED MapInvPlnt Project no. ANR-15-NMED-0002-02, by the Hypanema ANR Project no. ANR-12-BS03-003 and by ANR-11-LABX-0040-CIMI within the program ANR-11-IDEX-0002-02 within the thematic trimester on image processing.

Qi Wei and Simon Godsill are with Department of Engineering, University of Cambridge, CB2 1PZ, Cambridge, UK (e-mail: {qi.wei, sjg}@eng.cam.ac.uk).

Nicolas Dobigeon and Jean-Yves Tourneret are with University of Toulouse, IRIT/INP-ENSEEIH, 2 rue Camichel, BP 7122, 31071 Toulouse cedex 7, France (e-mail: {nicolas.dobigeon, jean-yves.tourneret}@enseeiht.fr).

José Bioucas-Dias is with Instituto de Telecomunicações and Instituto Superior Técnico, Universidade de Lisboa, Portugal (e-mail: {bioucas}@lx.it.pt).

## I. INTRODUCTION

### A. Background

The multi-band image fusion problem, i.e., fusing hyperspectral (HS) and multispectral (MS)/panchromatic (PAN) images has recently been receiving particular attention in remote sensing [2]. High spectral resolution multi-band imaging generally suffers from the limited spatial resolution of the data acquisition devices, mainly due to an unavoidable tradeoff between spatial and spectral sensitivities [3]. For example, HS images benefit from excellent spectroscopic properties with hundreds of bands but are limited by their relatively low spatial resolution compared to MS and PAN images (that are acquired in much fewer bands). As a consequence, reconstructing a high-spatial and high-spectral multi-band image from two degraded and complementary observed images is a challenging but crucial issue that has been addressed in various scenarios [4]–[7]. In particular, fusing a high-spatial low-spectral resolution image and a low-spatial high-spectral image is an archetypal instance of multi-band image reconstruction, such as pansharpening (MS+PAN) [8] or hyperspectral pansharpening (HS+PAN) [2]. Generally, the linear degradations applied to the observed images with respect to (w.r.t.) the target high-spatial and high-spectral image reduce to spatial and spectral transformations. Thus, the multi-band image fusion problem can be interpreted as restoring a three dimensional data-cube from two degraded data-cubes. A detailed formulation of this problem is presented in the next section.

### B. Problem Statement

This work directly follows the formulation of [1] and uses the well-admitted linear degradation model

$$\begin{aligned} \mathbf{Y}_L &= \mathbf{L}\mathbf{X} + \mathbf{N}_L \\ \mathbf{Y}_R &= \mathbf{X}\mathbf{B}\mathbf{S} + \mathbf{N}_R \end{aligned} \tag{1}$$

where

- $\mathbf{X} \in \mathbb{R}^{m_\lambda \times n}$  is the full resolution target image,
- $\mathbf{Y}_L \in \mathbb{R}^{n_\lambda \times n}$  and  $\mathbf{Y}_R \in \mathbb{R}^{m_\lambda \times m}$  are the observed spectrally degraded and spatially degraded images,
- $\mathbf{L} \in \mathbb{R}^{n_\lambda \times m_\lambda}$  is the spectral response of the sensor,
- $\mathbf{B} \in \mathbb{R}^{n \times n}$  is a cyclic convolution operator on the bands,

- $\mathbf{S} \in \mathbb{R}^{n \times m}$  is a  $d$  uniform downsampling operator, which has  $m = n/d$  ones on the block diagonal and zeros elsewhere, such that  $\mathbf{S}^H \mathbf{S} = \mathbf{I}_m$ ,
- $\mathbf{N}_L \in \mathbb{R}^{n_\lambda \times n}$  and  $\mathbf{N}_R \in \mathbb{R}^{m_\lambda \times m}$  are additive noise terms that are assumed to be distributed according to the following matrix normal distributions [9]

$$\begin{aligned}\mathbf{N}_L &\sim \mathcal{MN}_{n_\lambda, n}(\mathbf{0}_{n_\lambda, n}, \mathbf{\Lambda}_L, \mathbf{I}_n) \\ \mathbf{N}_R &\sim \mathcal{MN}_{m_\lambda, m}(\mathbf{0}_{m_\lambda, m}, \mathbf{\Lambda}_R, \mathbf{I}_m)\end{aligned}$$

and the matrices  $\mathbf{\Lambda}_L$  and  $\mathbf{\Lambda}_R$  are the noise covariance matrices depending on the sensors. Note that  $n_\lambda$  and  $m_\lambda$  are the numbers of bands in  $\mathbf{Y}_L$  and  $\mathbf{Y}_R$  and that  $n$  and  $m$  are the numbers of pixels per band in  $\mathbf{Y}_L$  and  $\mathbf{Y}_R$ .

Computing the maximum likelihood (ML) or the Bayesian estimators (associated with any prior) is a challenging task, mainly due to the large size of  $\mathbf{X}$  and to the presence of the downsampling operator  $\mathbf{S}$ , which prevents any direct use of the Fourier transform (FT) to diagonalize the joint spatial degradation operator  $\mathbf{BS}$ . To overcome this difficulty, several computational strategies have been designed to approximate the estimators. One strategy is using the Markov chain Monte Carlo (MCMC) algorithm to generate samples asymptotically distributed according to the posterior distribution of  $\mathbf{X}$  [10]. Despite this formal appeal, MCMC-based methods have the major drawback of being computationally expensive, which prevents their effective use when processing images of large size. Another strategy developed in [11] exploited a block coordinate descent method (BCD) to compute the maximum a posterior (MAP) estimator of  $\mathbf{X}$ , greatly decreasing the complexity compared to its MCMC counterpart. Based on a prior built from a sparse representation, the fusion problem was solved in [12], [13] with the split augmented Lagrangian shrinkage algorithm (SALSA) [14]. In [1], contrary to the algorithms described above, a much more efficient method was proposed to solve explicitly an underlying Sylvester equation (SE) derived from (1), leading to an algorithm referred to as Fast fUision based on Sylvester Equation (FUSE). This algorithm can be implemented *per se* to compute the ML estimator efficiently and has also the great advantage of being easily generalizable within a Bayesian framework when considering various priors (see the corresponding technical report [15] with more experimental results). The MAP estimators associated with a Gaussian prior similar to [10], [11] can be directly computed thanks to the proposed strategy. When handling more complex priors such as [12],

[13], the FUSE solution can be conveniently embedded within a conventional ADMM or a BCD algorithm. Although the FUSE algorithm has significantly accelerated the fusion of multi-band images, it requires the non-trivial assumption that the blurring matrix  $\mathbf{B}$  is invertible, which is not always guaranteed in practice.

In this work, we propose a more robust version of FUSE algorithm, which is termed as R-FUSE. In this R-FUSE, the FT of the target image, instead of its blurring version as in [1], is computed explicitly by exploiting the Woodbury formula. A direct consequence of this modification is getting rid of the invertibility assumption for the blurring matrix  $\mathbf{B}$ . A side product of this modification is that the permutations conducted in the frequency domain (characterized by the matrix  $\mathbf{P}$  in [1]) are no longer required in the R-FUSE algorithm.

## II. PROBLEM FORMULATION

Since adjacent HS bands are known to be highly correlated, the columns of  $\mathbf{X}$  usually reside in a subspace whose dimension  $\tilde{m}_\lambda$  is much smaller than the number of bands  $m_\lambda$  [16], [17], i.e.,  $\mathbf{X} = \mathbf{H}\mathbf{U}$  where  $\mathbf{H}$  is a full column rank matrix and  $\mathbf{U} \in \mathbb{R}^{\tilde{m}_\lambda \times n}$  is the projection of  $\mathbf{X}$  onto the subspace spanned by the columns of  $\mathbf{H} \in \mathbb{R}^{m_\lambda \times \tilde{m}_\lambda}$ .

According to the maximum likelihood or least squares principles, the fusion problem associated with the linear model (1) can be formulated as

$$\arg \min_{\mathbf{U}} L(\mathbf{U}) \quad (2)$$

where

$$L(\mathbf{U}) = \|\mathbf{\Lambda}_R^{-\frac{1}{2}} (\mathbf{Y}_R - \mathbf{H}\mathbf{U}\mathbf{B}\mathbf{S})\|_F^2 + \|\mathbf{\Lambda}_L^{-\frac{1}{2}} (\mathbf{Y}_L - \mathbf{L}\mathbf{H}\mathbf{U})\|_F^2$$

and  $\|\cdot\|_F$  represents the Frobenius norm.

## III. ROBUST FAST FUSION SCHEME

### A. Sylvester equation

Minimizing (2) w.r.t.  $\mathbf{U}$  is equivalent to force the derivative of  $L(\mathbf{U})$  to be zero, i.e.,  $\nabla L(\mathbf{U}) = 0$ , leading to the following matrix equation

$$\begin{aligned} & \mathbf{H}^H \mathbf{\Lambda}_R^{-1} \mathbf{H}\mathbf{U}\mathbf{B}\mathbf{S} (\mathbf{B}\mathbf{S})^H + \left( (\mathbf{L}\mathbf{H})^H \mathbf{\Lambda}_L^{-1} \mathbf{L}\mathbf{H} \right) \mathbf{U} \\ & = \mathbf{H}^H \mathbf{\Lambda}_R^{-1} \mathbf{Y}_R (\mathbf{B}\mathbf{S})^H + (\mathbf{L}\mathbf{H})^H \mathbf{\Lambda}_L^{-1} \mathbf{Y}_L. \end{aligned} \quad (3)$$

As mentioned in Section I-B, the difficulty for solving (3) results from the high dimensionality of  $\mathbf{U}$  and the presence of the downsampling matrix  $\mathbf{S}$ . The work in [1] showed that Eq. (3) can be solved analytically with two assumptions

- The blurring matrix  $\mathbf{B}$  is a block circulant matrix with circulant blocks.
- The decimation matrix  $\mathbf{S}$  corresponds to downsampling the original image and its conjugate transpose  $\mathbf{S}^H$  interpolates the decimated image with zeros.

As a consequence, the matrix  $\mathbf{B}$  can be decomposed as  $\mathbf{B} = \mathbf{F}\mathbf{D}\mathbf{F}^H$  with  $\mathbf{B}^H = \mathbf{F}\mathbf{D}^*\mathbf{F}^H$ , where  $\mathbf{F} \in \mathbb{R}^{n \times n}$  is the discrete Fourier transform (DFT) matrix ( $\mathbf{F}\mathbf{F}^H = \mathbf{F}^H\mathbf{F} = \mathbf{I}_n$ ),  $\mathbf{D} \in \mathbb{R}^{n \times n}$  is a diagonal matrix and  $*$  represents the conjugate operator. Another non-trivial assumption used in [1] is that the matrix  $\mathbf{D}$  (or equivalently  $\mathbf{B}$ ) is invertible, which is not necessary in this work as shown in Section III-B. In practice, the matrix  $\mathbf{D}$  is often non-invertible as the deconvolution is an ill-posed problem [18], [19]. The decimation matrix satisfies the property  $\mathbf{S}^H\mathbf{S} = \mathbf{I}_m$  and the matrix  $\underline{\mathbf{S}} \triangleq \mathbf{S}\mathbf{S}^H$  is symmetric and idempotent, i.e.,  $\underline{\mathbf{S}} = \underline{\mathbf{S}}^H$  and  $\underline{\mathbf{S}}\underline{\mathbf{S}}^H = \underline{\mathbf{S}}$ . For a practical implementation, multiplying an image by  $\underline{\mathbf{S}}$  can be achieved by doing entry-wise multiplication with an  $n \times n$  mask matrix with ones in the sampled position and zeros elsewhere.

After multiplying (3) on both sides by  $(\mathbf{H}^H \mathbf{\Lambda}_R^{-1} \mathbf{H})^{-1}$ , we obtain

$$\mathbf{C}_1 \mathbf{U} + \mathbf{U} \mathbf{C}_2 = \mathbf{C} \quad (4)$$

where

$$\mathbf{C}_1 = (\mathbf{H}^H \mathbf{\Lambda}_R^{-1} \mathbf{H})^{-1} \left( (\mathbf{LH})^H \mathbf{\Lambda}_L^{-1} \mathbf{LH} \right)$$

$$\mathbf{C}_2 = \mathbf{B} \underline{\mathbf{S}} \mathbf{B}^H$$

$$\mathbf{C} = (\mathbf{H}^H \mathbf{\Lambda}_R^{-1} \mathbf{H})^{-1} \left( \mathbf{H}^H \mathbf{\Lambda}_R^{-1} \mathbf{Y}_R (\mathbf{BS})^H + (\mathbf{LH})^H \mathbf{\Lambda}_L^{-1} \mathbf{Y}_L \right). \quad (5)$$

Eq. (4) is a Sylvester matrix equation that admits a unique solution if and only if an arbitrary sum of the eigenvalues of  $\mathbf{C}_1$  and  $\mathbf{C}_2$  is not equal to zero [20].

### B. Proposed closed-form solution

Using the eigen-decomposition  $\mathbf{C}_1 = \mathbf{Q}\mathbf{\Lambda}\mathbf{Q}^{-1}$  and multiplying both sides of (4) by  $\mathbf{Q}^{-1}$  leads to

$$\mathbf{\Lambda}\mathbf{Q}^{-1}\mathbf{U} + \mathbf{Q}^{-1}\mathbf{U}\mathbf{C}_2 = \mathbf{Q}^{-1}\mathbf{C}. \quad (6)$$

Right multiplying (6) by the DFT matrix  $\mathbf{F}$  on both sides and using the definitions of matrices  $\mathbf{C}_2$  and  $\mathbf{B}$  yields

$$\mathbf{\Lambda}\mathbf{Q}^{-1}\mathbf{U}\mathbf{F} + \mathbf{Q}^{-1}\mathbf{U}\mathbf{F}(\mathbf{D}\mathbf{F}^H\mathbf{S}\mathbf{F}\mathbf{D}^*) = \mathbf{Q}^{-1}\mathbf{C}\mathbf{F}. \quad (7)$$

Note that  $\mathbf{U}\mathbf{F} \in \mathbb{R}^{\tilde{m}_\lambda \times n}$  is the FT of the target image, which is a complex matrix. Eq. (7) can be regarded as an SE w.r.t.  $\mathbf{Q}^{-1}\mathbf{U}\mathbf{F}$ , which has a simpler form compared to (4) as  $\mathbf{\Lambda}$  is a diagonal matrix. Instead of using any block permutation matrix as in [1], we propose to solve the SE (7) row-by-row (i.e., band-by-band). Recall the following lemma originally proposed in [1].

**Lemma 1** (Wei *et al.*, [1]). *The following equality holds*

$$\mathbf{F}^H\mathbf{S}\mathbf{F} = \frac{1}{d}\mathbf{J}_d \otimes \mathbf{I}_m \quad (8)$$

where  $\mathbf{F}$  and  $\mathbf{S}$  are defined as in Section III-A,  $\mathbf{J}_d$  is the  $d \times d$  matrix of ones and  $\mathbf{I}_m$  is the  $m \times m$  identity matrix.

By simply decomposing the matrix  $\mathbf{J}_d$  as  $\mathbf{J}_d = \mathbf{1}_d\mathbf{1}_d^T$ , where  $\mathbf{1}_d \in \mathbb{R}^d$  is a vector of ones and using the mixed-product property of Kronecker product, i.e.,  $(\mathbf{A}_1\mathbf{A}_2) \otimes (\mathbf{A}_3\mathbf{A}_4) = (\mathbf{A}_1 \otimes \mathbf{A}_3)(\mathbf{A}_2 \otimes \mathbf{A}_4)$  (if  $\mathbf{A}_1, \mathbf{A}_2, \mathbf{A}_3$  and  $\mathbf{A}_4$  are matrices of proper sizes), we can easily get the following result

$$\mathbf{F}^H\mathbf{S}\mathbf{F} = \frac{1}{d}(\mathbf{1}_d \otimes \mathbf{I}_m)(\mathbf{1}_d^T \otimes \mathbf{I}_m) \quad (9)$$

Substituting (9) into (7) leads to

$$\mathbf{\Lambda}\bar{\mathbf{U}} + \bar{\mathbf{U}}\mathbf{M} = \bar{\mathbf{C}} \quad (10)$$

where  $\bar{\mathbf{U}} = \mathbf{Q}^{-1}\mathbf{U}\mathbf{F}$ ,  $\mathbf{M} = \frac{1}{d}\bar{\mathbf{D}}\bar{\mathbf{D}}^H$ ,  $\bar{\mathbf{D}} = \mathbf{D}(\mathbf{1}_d \otimes \mathbf{I}_m)$ ,  $\bar{\mathbf{C}} = \mathbf{Q}^{-1}\mathbf{C}\mathbf{F}$ . Eq. (10) is an SE w.r.t.  $\bar{\mathbf{U}}$  whose solution is significantly easier than the one of (6), due to the simple structure of the matrix  $\mathbf{M}$ . To ease the notation, the diagonal matrices  $\mathbf{\Lambda}$  and  $\mathbf{D}$  are rewritten as

$\Lambda = \text{diag}(\lambda_1, \dots, \lambda_{\tilde{m}_\lambda})$  and  $\mathbf{D} = \text{diag}(\mathbf{D}_1, \dots, \mathbf{D}_d)$ , where  $\text{diag}(\cdot_1, \dots, \cdot_k)$  represents a (block) diagonal matrix whose (block) diagonal elements are  $\cdot_1, \dots, \cdot_k$  and  $\lambda_i \geq 0, \forall i$ . Thus, we have  $\bar{\mathbf{D}}^H \bar{\mathbf{D}} = \sum_{t=1}^d \mathbf{D}_t^H \mathbf{D}_t = \sum_{t=1}^d \mathbf{D}_t^2$ .

In the following, we will show that (10) can be solved row-by-row explicitly. First, we rewrite  $\bar{\mathbf{U}}$  and  $\bar{\mathbf{C}}$  as  $\bar{\mathbf{U}} = [\bar{\mathbf{u}}_1^T, \dots, \bar{\mathbf{u}}_{\tilde{m}_\lambda}^T]^T$  and  $\bar{\mathbf{C}} = [\bar{\mathbf{c}}_1^T, \dots, \bar{\mathbf{c}}_{\tilde{m}_\lambda}^T]^T$ , where  $\bar{\mathbf{u}}_i \in \mathbb{R}^{1 \times n}$  and  $\bar{\mathbf{c}}_i \in \mathbb{R}^{1 \times n}$  are row vectors. Using these notations, (10) can be decomposed as

$$\lambda_i \bar{\mathbf{u}}_i + \bar{\mathbf{u}}_i \mathbf{M} = \bar{\mathbf{c}}_i$$

for  $i = 1, \dots, \tilde{m}_\lambda$ . Direct computation leads to

$$\bar{\mathbf{u}}_i = \bar{\mathbf{c}}_i (\mathbf{M} + \lambda_i \mathbf{I}_n)^{-1}. \quad (11)$$

Following the Woodbury formula [21] and using  $\bar{\mathbf{D}}^H \bar{\mathbf{D}} = \sum_{t=1}^d \mathbf{D}_t^2$ , the inversion in (11) can be easily computed as  $(\mathbf{M} + \lambda_i \mathbf{I}_n)^{-1} = \lambda_i^{-1} \mathbf{I}_n - \lambda_i^{-1} \bar{\mathbf{D}} \left( \lambda_i d \mathbf{I}_m + \sum_{t=1}^d \mathbf{D}_t^2 \right)^{-1} \bar{\mathbf{D}}^H$ . As  $\lambda_i d \mathbf{I}_m + \sum_{t=1}^d \mathbf{D}_t^2$  is a real diagonal matrix, its inversion is easy to be computed with a complexity of order  $\mathcal{O}(m)$ . Using this simple inversion, the solution  $\bar{\mathbf{U}}$  of the SE (10) can be computed row-by-row (band-by-band) as

$$\bar{\mathbf{u}}_i = \lambda_i^{-1} \bar{\mathbf{c}}_i - \lambda_i^{-1} \bar{\mathbf{c}}_i \bar{\mathbf{D}} \left( \lambda_i d \mathbf{I}_m + \sum_{t=1}^d \mathbf{D}_t^2 \right)^{-1} \bar{\mathbf{D}}^H \quad (12)$$

for  $i = 1, \dots, \tilde{m}_\lambda$ . The final estimator of  $\mathbf{X}$  is obtained as

$$\hat{\mathbf{X}} = \mathbf{H} \mathbf{Q} \bar{\mathbf{U}} \mathbf{F}^H.$$

### C. Difference with [1]

It is interesting to mention some important differences between the proposed R-FUSE strategy and the one of [1]:

- The matrix  $\mathbf{B}$  (or  $\mathbf{D}$ ) is not required to be invertible.
- Each band can be restored as a whole instead of block-by-block ( $d$  blocks).

Algorithm 1 summarizes the derived R-FUSE steps required to calculate the estimated image  $\hat{\mathbf{X}}$ , where the different parts with [1] have been highlighted in red.

---

**Algorithm 1: Robust Fast fUision based on solving a Sylvester Equation (R-FUSE)**


---

**Input:**  $\mathbf{Y}_L, \mathbf{Y}_R, \mathbf{\Lambda}_L, \mathbf{\Lambda}_R, \mathbf{L}, \mathbf{B}, \mathbf{S}, \mathbf{H}, d$   
1  $\mathbf{D} \leftarrow \text{EigDec}(\mathbf{B});$  // FFT transformation  
2  $\bar{\mathbf{D}} \leftarrow \mathbf{D}(\mathbf{1}_d \otimes \mathbf{I}_m);$   
3  $\mathbf{C}_1 \leftarrow \mathbf{C}_1(\mathbf{H}, \mathbf{L}, \mathbf{\Lambda}_L, \mathbf{\Lambda}_R);$  // Compute cf. (5)  
4  $(\mathbf{Q}, \mathbf{\Lambda}) \leftarrow \text{EigDec}(\mathbf{C}_1);$  // cf.  $\mathbf{C}_1 = \mathbf{Q}\mathbf{\Lambda}\mathbf{Q}^{-1}$   
5  $\mathbf{C} \leftarrow \mathbf{C}(\mathbf{H}, \mathbf{L}, \mathbf{\Lambda}_L, \mathbf{\Lambda}_R, \mathbf{Y}_L, \mathbf{Y}_R, \mathbf{B}, \mathbf{S});$  // cf. (5)  
6  $\bar{\mathbf{C}} \leftarrow \mathbf{Q}^{-1}\mathbf{C}\mathbf{F};$   
// Compute  $\bar{\mathbf{U}}$  band by band ( $\tilde{m}_\lambda$  bands)  
7 **for**  $l = 1$  **to**  $\tilde{m}_\lambda$  **do**  
8 |  $\bar{\mathbf{u}}_i \leftarrow \bar{\mathbf{u}}_i(\lambda_i, d, \bar{\mathbf{c}}_i, \bar{\mathbf{D}}, \mathbf{D});$  // cf. (12)  
9 **end**  
10 **Set**  $\hat{\mathbf{X}} = \mathbf{H}\mathbf{Q}\bar{\mathbf{U}}\mathbf{F}^H;$   
**Output:**  $\hat{\mathbf{X}}$

---

#### D. Complexity Analysis

The most computationally expensive part of the proposed algorithm is the computation of the matrix  $\bar{\mathbf{C}}$  (because of the FFT and iFFT operations), which has a complexity of order  $\mathcal{O}(\tilde{m}_\lambda n \log n)$ . The left matrix multiplications with  $\mathbf{Q}^{-1}$  (to compute  $\bar{\mathbf{C}}$ ) and with  $(\mathbf{H}^H \mathbf{\Lambda}_R^{-1} \mathbf{H})^{-1}$  (to compute  $\mathbf{C}$ ) have a complexity of order  $\mathcal{O}(\tilde{m}_\lambda^2 n)$ . Thus, the calculation of  $\bar{\mathbf{C}}$  has a total complexity of order  $\mathcal{O}(\tilde{m}_\lambda n \cdot \max\{\log n, \tilde{m}_\lambda\})$ , which can be approximated by  $\mathcal{O}(\tilde{m}_\lambda n \log n)$  as  $\log n \gg \tilde{m}_\lambda$ .

Note that the proposed R-FUSE scheme can be embedded within an ADMM or a BCD algorithm to deal with Bayesian estimators, as explained in [1].

## IV. EXPERIMENTAL RESULTS

This section applies the proposed fusion method to two Bayesian fusion schemes (with appropriate priors for the unknown matrix  $\mathbf{X}$ ) that have been investigated in [11] and [12]. Note that these two methods require to solve a minimization problem similar to (2). All the algorithms have been implemented using MATLAB R2015b on a computer with Intel(R) Core(TM) i7-4790 CPU@3.60GHz and 16GB RAM.

### A. Fusion Quality Metrics

Following [1], we used the restored signal-to-noise ratio (RSNR), the averaged spectral angle mapper (SAM), the universal image quality index (UIQI), the relative dimensionless global error in synthesis (ERGAS) and the degree of distortion (DD) as quantitative measures

to evaluate the quality of the fused results. The larger RSNR and UIQI, or the smaller SAM, ERGAS and DD, the better the fusion.

### B. Fusion of Multi-band images

The reference image considered here as the high-spatial and high-spectral image is a  $512 \times 256 \times 93$  HS image acquired over Pavia, Italy, by the reflective optics system imaging spectrometer (ROSIS). This image was initially composed of 115 bands that have been reduced to 93 bands after removing the water vapor absorption bands. A composite color image of the scene of interest is shown in Fig. 1 (right).

First,  $\mathbf{Y}_R$  has been generated by applying a  $5 \times 5$  Gaussian filter (shown in the left of Figs. 5) and by down-sampling every 4 pixels in both vertical and horizontal directions for each band of the reference image. Second, a 4-band MS image  $\mathbf{Y}_L$  has been obtained by filtering  $\mathbf{X}$  with the LANDSAT-like reflectance spectral responses [22]. The HS and MS images are both contaminated by zero-mean additive Gaussian noises with  $\text{SNR}_H = 40\text{dB}$  for HS bands and  $\text{SNR}_M = 30\text{dB}$  for MS bands. The observed HS and MS images are shown in Fig. 1 (left and middle).

We consider the Bayesian fusion with Gaussian [10] and total variation (TV) [12] priors that were considered in [1]. The subspace matrix  $\mathbf{H}$  was estimated using PCA as in [1]. The proposed R-FUSE and FUSE algorithms are compared in terms of their performance and computational time for the same optimization problem (corresponding to (18) in [1]). The estimated images obtained with the different algorithms are depicted in Fig. 2 and are visually very similar. The corresponding quantitative results are reported in Table I and confirm the same performance of FUSE and R-FUSE in terms of the various fusion quality measures (RSNR, UIQI, SAM, ERGAS and DD). Note that the results associated with a TV prior are slightly better than the ones obtained with a Gaussian prior, which can be attributed to the well-known denoising property of the TV prior. A particularity of the R-FUSE algorithm is its reduced computational complexity due to the avoidance of any permutation in the frequency domain when solving the Sylvester matrix equation, as demonstrated by the computational time also reported in Table I.



Fig. 1. Pavia dataset: HS image (left), MS image (middle) and reference image (right).



Fig. 2. HS+MS fusion results. 1st: FUSE using Gaussian prior, 2nd: R-FUSE using Gaussian prior, 3rd: FUSE using TV prior and 4th: R-FUSE using TV prior.

### *C. More results on other datasets*

We have tested all the algorithms on other datasets for fusing an HS image and a PAN image. The reference image is a  $392 \times 180 \times 176$  HS image obtained over Moffett field, CA, in 1994 by the JPL/NASA airborne visible/infrared imaging spectrometer (AVIRIS). This image was initially composed of 224 bands and have been reduced to 176 bands after removing the water vapor absorption bands. A composite color image of the scene of interest

TABLE I  
PERFORMANCE OF HS+MS FUSION METHODS: RSNR (IN DB), UIQI, SAM (IN DEGREE), ERGAS, DD (IN  $10^{-3}$ )  
AND TIME (IN SECOND).

| Prior    | Methods | RSNR   | UIQI   | SAM   | ERGAS | DD    | Time        |
|----------|---------|--------|--------|-------|-------|-------|-------------|
| Gaussian | FUSE    | 29.243 | 0.9904 | 1.513 | 0.902 | 6.992 | 0.27        |
|          | R-FUSE  | 29.243 | 0.9904 | 1.513 | 0.902 | 6.992 | <b>0.24</b> |
| TV       | FUSE    | 29.629 | 0.9914 | 1.456 | 0.853 | 6.761 | 133         |
|          | R-FUSE  | 29.629 | 0.9914 | 1.456 | 0.853 | 6.761 | <b>115</b>  |

is shown in Fig. 3 (right). The HS image has been generated by applying a  $5 \times 5$  Gaussian filter on each band of the reference image. Besides, a PAN image is obtained by successively averaging the adjacent bands in visible bands (1 ~ 41 bands) according to realistic spectral responses. In addition, the HS and PAN images have been both contaminated by zero-mean additive Gaussian noises. The SNR of the HS image is 40dB for all the bands and the SNR of the PAN image is 30dB. The HS and PAN images are shown in the left and middle of Fig. 3. The results are displayed in Fig. 4 whereas more quantitative results are reported in Table II. These results confirm that the proposed R-FUSE algorithm can achieve the same performance as the FUSE one with the advantage of reducing the computation time.



Fig. 3. Moffett field dataset: HS image (left), PAN image (middle) and reference image (right).



Fig. 4. HS+PAN fusion results. 1st: FUSE using Gaussian prior, 2nd: R-FUSE using Gaussian prior, 3rd: FUSE using TV prior and 4th: R-FUSE using TV prior.

TABLE II  
PERFORMANCE OF HS+PAN FUSION METHODS: RSNR (IN DB), UIQI, SAM (IN DEGREE), ERGAS, DD (IN  $10^{-2}$ ) AND TIME (IN SECOND).

| Prior    | Methods | RSNR   | UIQI   | SAM   | ERGAS | DD    | Time        |
|----------|---------|--------|--------|-------|-------|-------|-------------|
| Gaussian | FUSE    | 18.684 | 0.9804 | 4.897 | 3.548 | 1.290 | 0.29        |
|          | R-FUSE  | 18.684 | 0.9804 | 4.897 | 3.548 | 1.290 | <b>0.26</b> |
| TV       | FUSE    | 18.824 | 0.9810 | 4.500 | 3.495 | 1.213 | 180         |
|          | R-FUSE  | 18.824 | 0.9810 | 4.500 | 3.495 | 1.213 | <b>166</b>  |

#### D. Robustness w.r.t. the blurring kernel

In this section, we consider a kernel similar to the one used in Section IV-B, which is displayed in the middle of Fig. 5 (the difference between the two kernels is shown in the right). Note that this trivial change makes the Fourier transform of the new kernel have some values that are very close to zero. Due to the inversion of  $\mathbf{B}$  in FUSE, this slight change can dramatically impact the performance of the FUSE algorithm. The fusion performance of FUSE and R-FUSE with a TV prior is summarized in Table III. Obviously, the performance of FUSE degrades a lot due to the presence of close-to-zero values in the kernel FT, which does not agree with the invertibility assumption of  $\mathbf{B}$ . On the contrary, the proposed R-FUSE provides results very close to (almost the same with) those obtained in Section IV-B,

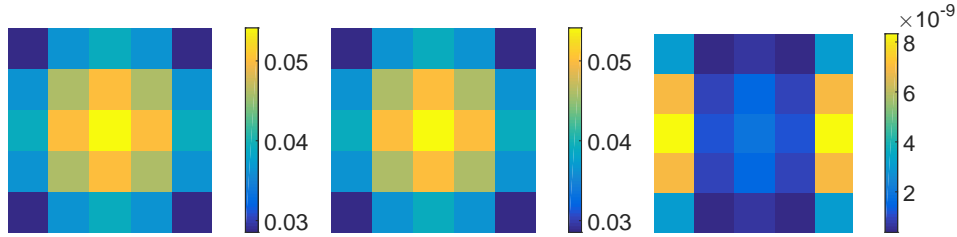


Fig. 5. Blurring kernel used in Section IV-B (left), in this section (middle) and their difference (right).

TABLE III  
PERFORMANCE OF HS+MS FUSION METHODS WITH A SLIGHTLY DIFFERENT KERNEL: RSNR (IN DB), UIQI, SAM (IN DEGREE), ERGAS, DD (IN  $10^{-3}$ ) AND TIME (IN SECOND).

| Prior | Methods | RSNR   | UIQI   | SAM   | ERGAS | DD    | Time |
|-------|---------|--------|--------|-------|-------|-------|------|
| TV    | FUSE    | 9.985  | 0.5640 | 14.50 | 8.348 | 74.7  | 133  |
|       | R-FUSE  | 29.629 | 0.9914 | 1.456 | 0.853 | 6.761 | 115  |

demonstrating its robustness w.r.t. the blurring kernel.

## V. CONCLUSION

This paper developed a new robust and faster multi-band image fusion method based on the resolution of a generalized Sylvester equation. The application of the Woodbury formula allows any permutation in the frequency domain to be avoided and brings two benefits. First, the invertibility assumption of the blurring operator is not necessary, leading to a more robust fusion strategy. Second, the computational complexity of the fusion algorithm is reduced. Similar to the method in [1], the proposed algorithm can be embedded into a block coordinate descent or an alternating direction method of multipliers to implement (hierarchical) Bayesian fusion models. Numerical experiments confirmed that the proposed robust fast fusion method has the advantage of reducing the computational cost and also is more robust to the blurring kernel conditioning, compared with the method investigated in [1].

## REFERENCES

- [1] Q. Wei, N. Dobigeon, and J.-Y. Tourneret, "Fast fusion of multi-band images based on solving a Sylvester equation," *IEEE Trans. Image Process.*, vol. 24, no. 11, pp. 4109–4121, Nov. 2015.
- [2] L. Loncan, L. B. Almeida, J. M. Bioucas-Dias, X. Briottet, J. Chanussot, N. Dobigeon, S. Fabre, W. Liao, G. Licciardi, M. Simoes, J.-Y. Tourneret, M. Veganzones, G. Vivone, Q. Wei, and N. Yokoya, "Hyperspectral pansharpening: a review," *IEEE Geosci. Remote Sens. Mag.*, vol. 3, no. 3, pp. 27–46, Sept. 2015.

- [3] C.-I. Chang, *Hyperspectral data exploitation: theory and applications*. New York: John Wiley & Sons, 2007.
- [4] H. Aanaes, J. Sveinsson, A. Nielsen, T. Bovith, and J. Benediktsson, "Model-based satellite image fusion," *IEEE Trans. Geosci. Remote Sens.*, vol. 46, no. 5, pp. 1336–1346, May 2008.
- [5] T. Stathaki, *Image fusion: algorithms and applications*. New York: Academic Press, 2011.
- [6] M. Gong, Z. Zhou, and J. Ma, "Change detection in synthetic aperture radar images based on image fusion and fuzzy clustering," *IEEE Trans. Image Process.*, vol. 21, no. 4, pp. 2141–2151, Apr. 2012.
- [7] A. P. James and B. V. Dasarathy, "Medical image fusion: A survey of the state of the art," *Information Fusion*, vol. 19, pp. 4–19, 2014.
- [8] B. Aiazzi, L. Alparone, S. Baronti, A. Garzelli, and M. Selva, "25 years of pansharpening: a critical review and new developments," in *Signal and Image Processing for Remote Sensing*, 2nd ed., C. H. Chen, Ed. Boca Raton, FL: CRC Press, 2011, ch. 28, pp. 533–548.
- [9] A. Gupta and D. Nagar, *Matrix Variate Distributions*, ser. Monographs and Surveys in Pure and Applied Mathematics. Taylor & Francis, 1999.
- [10] Q. Wei, N. Dobigeon, and J.-Y. Tourneret, "Bayesian fusion of multi-band images," *IEEE J. Sel. Topics Signal Process.*, vol. 9, no. 6, pp. 1117–1127, Sept. 2015.
- [11] —, "Bayesian fusion of multispectral and hyperspectral images using a block coordinate descent method," in *Proc. IEEE GRSS Workshop Hyperspectral Image Signal Process.: Evolution in Remote Sens. (WHISPERS)*, Tokyo, Japan, Jun. 2015.
- [12] M. Simoes, J. Bioucas-Dias, L. Almeida, and J. Chanussot, "A convex formulation for hyperspectral image superresolution via subspace-based regularization," *IEEE Trans. Geosci. Remote Sens.*, vol. 53, no. 6, pp. 3373–3388, Jun. 2015.
- [13] Q. Wei, J. Bioucas-Dias, N. Dobigeon, and J. Tourneret, "Hyperspectral and multispectral image fusion based on a sparse representation," *IEEE Trans. Geosci. Remote Sens.*, vol. 53, no. 7, pp. 3658–3668, Jul. 2015.
- [14] M. Afonso, J. M. Bioucas-Dias, and M. Figueiredo, "An augmented Lagrangian approach to the constrained optimization formulation of imaging inverse problems," *IEEE Trans. Image Process.*, vol. 20, no. 3, pp. 681–95, 2011.
- [15] Q. Wei, N. Dobigeon, and J.-Y. Tourneret, "Fast fusion of multi-band images based on solving a Sylvester equation – Complementary results and supporting materials," Univ. of Toulouse, IRIT/INP-ENSEEIH, Tech. Rep., Jun. 2015. [Online]. Available: <http://wei.perso.enseeiht.fr/papers/2015-WEI-TR-Sylvester.pdf>
- [16] C.-I. Chang, X.-L. Zhao, M. L. Althouse, and J. J. Pan, "Least squares subspace projection approach to mixed pixel classification for hyperspectral images," *IEEE Trans. Geosci. Remote Sens.*, vol. 36, no. 3, pp. 898–912, 1998.
- [17] J. M. Bioucas-Dias and J. M. Nascimento, "Hyperspectral subspace identification," *IEEE Trans. Geosci. Remote Sens.*, vol. 46, no. 8, pp. 2435–2445, 2008.
- [18] R. Neelamani, H. Choi, and R. Baraniuk, "ForWaRD: Fourier-wavelet regularized deconvolution for ill-conditioned systems," *IEEE Trans. Signal Process.*, vol. 52, no. 2, pp. 418–433, Feb 2004.
- [19] Y. Wang, J. Yang, W. Yin, and Y. Zhang, "A new alternating minimization algorithm for total variation image reconstruction," *SIAM J. Imaging Sci.*, vol. 1, no. 3, pp. 248–272, 2008.
- [20] R. H. Bartels and G. Stewart, "Solution of the matrix equation  $AX + XB = C$ ," *Communications of the ACM*, vol. 15, no. 9, pp. 820–826, 1972.
- [21] M. A. Woodbury, "Inverting modified matrices," *Memorandum report*, vol. 42, p. 106, 1950.

- [22] D. Fleming, "Effect of relative spectral response on multi-spectral measurements and NDVI from different remote sensing systems," Ph.D. dissertation, University of Maryland, Department of Geography, USA, 2006.